energies

Article

Adaptive Backward/Forward Sweep for Solving Power Flow of Islanded Microgrids

Abhimanyu Kumar †, Abhishek Kumar †, Rammohan Mallipeddi * and Dong-Gyu Lee

Department of Artificial Intelligence, Kyungpook National University, Daehak-ro, Buk-gu, Daegu 41566, Republic of Korea
* Correspondence: mallipeddi.ram@gmail.com; Tel.: +82-10-3575-1276
† These authors contributed equally to this work.

Abstract: This paper presents an algorithm for solving the power flow (PF) problem of droop-regulated AC microgrids (DRACMs) operating in isolated mode. These systems are based on radial distribution networks without having a slack bus to facilitate conventional computations. Moreover, distributed generation units have to distribute the power and voltage regulation among themselves as a function of operating frequency and voltage droop rather than having a slack bus that regulates voltage and power demands. Based on the conventional backward/forward sweep algorithm (BFS), the proposed method is a derivative-free PF algorithm. To manage the absence of a slack bus in the system, the BFS algorithm introduces new loops, equations, and self-adaptation procedures to its computation procedures. A comparison is presented between the proposed BFS algorithm and other state-of-the-art PF algorithms, as well as PSCAD/EMTDC. In comparison to existing algorithms, the proposed approach is fast, simple, accurate, and easy to implement, and it can be considered an effective tool for planning and analyzing islanded DRACMs.

Keywords: islanded AC microgrid; backward/forward sweep algorithm; distributed generation; self-adaptation; power flow

Citation: Kumar, A.; Kumar, A.; Mallipeddi, R.; Lee, D.-G. Adaptive Backward/Forward Sweep for Solving Power Flow of Islanded Microgrids. *Energies* **2022**, *15*, 9348. https://doi.org/10.3390/en15249348

Academic Editor: Abu-Siada Ahmed

Received: 16 October 2022
Accepted: 4 December 2022
Published: 9 December 2022

1. Introduction

Load flow analysis has been required for the investigation, usual operation, control, and optimization of any distribution system. Tools and programs of load flow analysis have been in use for the operation and planning of distribution systems [1]. In system restoration and reconfiguration studies, load flow analysis tools have also been used [2]. For transmission systems, various classical load flow algorithms such as Gauss–Seidel, Newton–Raphson, and its variant the fast decoupled method have been proposed [3–7]. On the other hand, they become ineffective if the distribution system is ill-conditioned [8,9]. The BFS algorithm is preferable in such cases, as it is typically implemented for weakly meshed and radial distribution systems [9]. The computational equations of BFS are based on circuit laws such as KCL and KVL [9–11].

Due to the increased penetration of DGs in the distribution system, power can now flow in both directions which adds new dimensions to distribution system analysis [12]. A cluster of DGs can also behave as microgrids (MGs) and can also supply the required power for the demands of local loads without any assistance from the main grid. In other words, the operation of networks with DGs as microgrids (MGs) can provide a high reliability and efficiency in the distribution network in view of their islanded abilities. To ensure sufficient stability in an islanded microgrid (MG) mode of operation, the method of droop regulation is widely used. The droop regulation approach is comparatively simple and only consists of two equations of the droop function. In the droop regulation approach, a DG's generated real power can be modulated by its constant frequency droop coefficient, m_P, following the equation $\triangle f = m_P \triangle P_g$, which shows that any modification of the system frequency will produce a proportional shift of the active power generation in each DG [13]. Similarly, the second equation, $\triangle V = n_Q \triangle Q_g$, implies that a shift of the bus voltage would cause a proportionate adjustment in the reactive power generation in DGs according to the voltage droop coefficient, n_Q. These equations ensure that the difficulty of regulating the active and reactive load demand is easily tackled by shared loads in inverse proportion to the droop coefficients of all the DGs without using communication links.

MGs can operate in islanded mode when the system load is quite low; however, they return to the grid-connected mode when the system load surpasses the generation capacities of the connected DGs. A grid-connected MG is operated differently than an island-connected MG. For grid-connected DGs, the main grid regulates the system frequency for all DGs in a distribution system and can also be modeled as slack buses that provide the necessary energy to the system for compensating the extra burden from local loads and losses, while the buses connected to DGs are modeled as PQ buses that consider the generated power as a negative load. In this situation, conventional algorithms are applied for efficiently solving PF problems. There are two main classes of algorithms based on the Jacobian matrix requirement: (1) methods that use Jacobian matrices, such as the fast decoupled load flow and Newton–Raphson methods; and (2) approaches that avoid Jacobian matrices, such as backward/forward sweep (BFS) and approaches using node equations [14,15].

The droop characteristics of buses that are connected to DGs prevent them from being modeled as PV, PQ, or even slack buses in IDRACMs. Fast decoupled, Gauss–Seidel, Newton–Raphson, and BFS methods are conventional models of load flow that cannot cope with frequency as a variable, making them ineffective when it comes to the load flow problems of islanded MGs. Additionally, a change in the frequency of a system changes the impedance as well. It has been attempted in the literature to solve this problem by modifying different conventional PF techniques. These modifications were highlighted in [12,16], which employed them to resolve the load flow issue encountered with droop-controlled islanded MGs. The authors did not consider the droop equations in their procedures to define the slack, PQ, and PV buses, which was previously reported in [17]. The Newton trust-region algorithm was extended by Abdelaziz et al. [17] to accommodate DG droop characteristics when operating in the islanded mode. A nonlinear equation for the solution of the load flow problem is derived from the modeling of the droop, PV, and PQ buses. In [18], a modified Newton–Raphson (MNR) method took the droop characteristics of DGs into account when modifying Newton–Raphson. Slack buses were not required in this algorithm, and buses connected to droop-controlled DGs were treated as droop buses. This algorithm was accurate, but it required the inverse of the Jacobian matrix, which is computationally intensive.

Hence, the conventional procedure of the BFS algorithm needs to be revised in order to solve the load flow problem of IDRACMs. A recently published article in [19] considered several types of DGs, as well as the buses that were connected to these DGs. However, the algorithm could only be applied when the MG was grid-connected. An optimized direct backward/forward sweep (DBFS) algorithm was introduced in [20] for solving the islanded droop-controlled MG load flow problem. PQ buses were used to handle DGs in the proposed methodology. The magnitude of the voltage on one of the DG buses, however, was also selected as a global variable, similarly to the frequency.

A revised variant of the conventional BFS was presented in [21] to deal with the DG's droop and the lack of a reference bus. A virtual bus was attached to one of the DG buses and utilized as a reference bus. To achieve zero PF through VB after the BFS algorithm had converged, we needed to adjust the magnitude and frequency of the voltage in the section. Refs. [20,21] presented BFS algorithms that did not take into account DG droop characteristics and followed conventional algorithms. In both algorithms, the droop characteristics of DGs were only considered in the post-BFS step to update the reactive and real DG power generation, which decelerated the algorithm's convergence (voltage magnitude of DG buses and system frequency). In Table 1, we summarize recently published algorithms based on the above-mentioned three categories: optimization-based algorithms, Jacobian-based algorithms, and non-Jacobian algorithms.

Table 1. A summary of major PF algorithms of islanded DRACMs proposed recently.

Ref., Year	Title
	Optimization-based PF algorithm
[22], 2020	A Calculation Method for Three-Phase Power Flow in Micro-Grid Based on Smooth Function
[23], 2021	Power flow analysis of islanded microgrids: a differential evolution approach
	Jacobian-based PF algorithm
[24], 2020	A decoupled extended power flow analysis based on Newton-Raphson method for islanded microgrids
[25], 2020	A Nested-Iterative Newton-Raphson based Power Flow Formulation for Droop-based Islanded Microgrids
[26], 2020	Load flow calculation for droop-controlled islanded microgrids based on direct Newton–Raphson method with step size optimization
[27], 2020	Power flow approach based on the S-iteration process
[28], 2021	An Inversion-Free Robust Power-Flow Algorithm for Microgrids
[29], 2022	Comprehensive enhanced Newton Raphson approach for power flow analysis in droop-controlled islanded AC microgrids
[30], 2022	A novel three-phase unbalanced power flow solution for islanded microgrids with distributed generations under droop controls
[31], 2022	An algorithm for power flow analysis in isolated hybrid energy microgrid considering DG droop model and virtual impedance control loop
	Non-Jacobian-based PF algorithm
[32], 2020	A Backward/Forward Method for Solving Load Flows in Droop-Controlled Microgrids
[33], 2020	An inversion-free sparse Zbus power flow algorithm for large-scale droop controlled islanded microgrids
[34], 2021	An efficient iterative approach for power flow solution of droop-controlled islanded AC microgrids through conventional methods
[35], 2022	An Accurate Power Flow Method for Microgrids with Conventional Droop Control
[36], 2022	MANA-Based Load-Flow Solution for Islanded AC Microgrids

In this paper, we develop a modified variant of the BFS algorithm to enhance the convergence for the PF problem of islanded MGs. A major barrier to implementing conventional PF algorithms such as the BFS algorithm is the lack of a slack bus that can establish the voltage reference to be used in the algorithm for updating bus voltages and the distribution of power (summation of load and losses) by droop-controlled DGs. Due to the lack of a reference bus, the DGs provide the balance reactive power while allowing for fluctuations in the voltage of the buses.

Our method, however, remains simplistic after compensating for these issues. Unlike the conventional backward sweep, droop equations are considered in the backward sweep for calculating branch currents. We also modify the forward sweep to provide stability for the significant changes in voltage steps due to the changes in voltage levels. After the modified BFS algorithm has converged, we update the reference bus voltage and frequency. When the new voltage and frequency settings are introduced, the modified BFS algorithm is applied until the reference bus can meet its droop condition. The proposed algorithm effectively incorporates the droop parameters into the forward and backward sweeps to account for droop characteristics. The popular non-Jacobian PF algorithms, such as ABFS, DBFS, and MBFS, are compared with the proposed algorithm. To assess the effectiveness of the proposed algorithm, we also included Jacobian-type algorithms, PSCAD/EMTC, as part of the comparison analysis.

2. Modeling of Microgrid Components

For IDRACM, accurate models of the DGs and the loads are required to solve the PF problem effectively. Here, we discuss the mathematical models of systems loads and DGs utilized in this study.

2.1. Model of Line Impedance

In MGs, the lines are generally considered to be unbalanced. The equivalent reduced branch circuit can be estimated in an unbalanced case by Kron's reduction and Carson's equations. Since the operating frequency is not constant in the system, we have to consider frequency dependencies in the impedance model. We can express the line impedance between buses i and j, $[\mathbf{Z}_{ij}^{abc}]$, using the following equation:

$$[\mathbf{Z}_{ij}^{abc}(w)] = \begin{bmatrix} Z_{ij}^{aa-n}(w) & Z_{ij}^{ab-n}(w) & Z_{ij}^{ac-n}(w) \\ Z_{ij}^{ba-n}(w) & Z_{ij}^{bb-n}(w) & Z_{ij}^{bc-n}(w) \\ Z_{ij}^{ca-n}(w) & Z_{ij}^{cb-n}(w) & Z_{ij}^{cc-n}(w) \end{bmatrix}. \tag{1}$$

where $\mathbf{Z}_{ij}^{st-n}$ $(s, t \in \{a, b, c\})$ represents the line impedance between phases s and t of buses i and j, taking into account the neutral line. Here, w represents the operating frequency of the system.

2.2. System Load Voltage Dependency Model

Based on the system operating frequency characteristics and its static voltage dependency, the magnitude of the active and reactive load at bus i can be defined as follows:

$$\begin{aligned} P_{l,i} &= P_{l,i}^{0}\left(a_{p,i} + b_{p,i}|V_i| + c_{p,i}|V_i|^2 + d_{p,i}|V_i|^{e_{p,i}}\right) \\ Q_{l,i} &= Q_{l,i}^{0}\left(a_{q,i} + b_{q,i}|V_i| + c_{q,i}|V_i|^2 + d_{q,i}|V_i|^{e_{q,i}}\right), \end{aligned} \tag{2}$$

where $a_{p,i}$, $b_{p,i}$, $c_{p,i}$, $d_{p,i}$, $e_{p,i}$, $a_{q,i}$, $b_{q,i}$, $c_{q,i}$, $d_{q,i}$, and $e_{q,i}$ are referred to as load coefficients, which satisfy the following equation.

$$\begin{aligned} a_{p,i} + b_{p,i} + c_{p,i} + d_{p,i} + e_{p,i} = 1 \\ a_{q,i} + b_{q,i} + c_{q,i} + d_{q,i} + e_{q,i} = 1 \end{aligned} \tag{3}$$

The values $P_{l,i}^{0}$ and $Q_{l,i}^{0}$ indicate the nominal active and reactive loads, respectively.

2.3. Droop-Regulated Distributed Generations Model

Microgrids connected to the grid can utilize DGs to supply constant active and reactive power to satisfy local load requirements. Similar to conventional power systems, a slack bus (main grid) provides or observes the difference between a DG's generated power and total load demands. Consequently, the system's frequency and voltage at the slack bus are constantly maintained during operation. Accordingly, buses connected to DGs can be modeled as PV or PQ buses, just like traditional systems. The following reasons prevent us from modeling the DG's buses as PV or PQ buses in islanded operations.

(i) An absence of a slack bus in the system.
(ii) Due to their small size, any of the DGs cannot act as a slack bus to regulate and maintain a constant system frequency.
(iii) Mismatches between power production and demand could lead to deviations in voltage and frequency to reduce the mismatch to zero.
(iv) The absence of a reference for the frequency and voltage as there is no main grid.

Therefore, slack buses should not be taken into account when solving the PF problem for IDRACMs. To formulate the PF problem without slack buses, a new droop-controlled bus must be developed for islanded MGs. Consequently, when the DG bus has a constant power factor and constant voltage, a new droop bus is formulated for both the PQ and PV buses. The droop characteristics of controllers can be used to calculate the power-sharing between DG sources on these droop buses. In conventional networks, large synchronous generators perform similarly. Increases in active power and reactive power result in decreases in frequency and voltage amplitude, respectively, according to the droop controller characteristics. In the following droop-controlled bus, the PFs for active, reactive, and apparent power can be determined as follows:

$$S = E\angle\delta\left(\frac{(E\angle\delta - V)^*}{Z\angle\theta}\right), \tag{4}$$

where V and E represent the voltage at the common bus and output of the inverter, respectively; δ represents the angle between V and E; and Z and θ represent the line impedance's magnitude and phase angle, respectively. By assuming a small value of θ, active and reactive power can be estimated by the following equations.

$$P = \frac{V}{Z}((Ecos\,\delta - V)cos\,\theta + E\delta sin\,\theta) \tag{5}$$

$$Q = \frac{V}{Z}((Ecos\,\delta - V)sin\,\theta + E\delta cos\,\theta) \tag{6}$$

Due to the coupling inductor at the converter output, the output impedance of the converter is primarily inductive. Therefore, θ is close to 90°. Consequently, we can simplify Equations (5) and (6) to,

$$P = \frac{V}{Z}E\delta, \tag{7}$$

$$Q = \frac{V}{Z}(E - V) \tag{8}$$

The active power varies with the power angle, while the reactive power varies with the voltage magnitude as shown in Equations (7) and (8). This allows the active and reactive power to be adjusted independently by adjusting the output voltage and frequency of the inverter.

According to the $(P - \omega)$ and $(Q - V)$ droop controls, Equations (7) and (8) can be redefined as follows.

$$\omega = \omega^* - S_p P, \tag{9}$$

$$V = V^* - S_q Q, \tag{10}$$

where V^* and ω^* represent the nominal voltage magnitude and nominal operating frequency, respectively; S_q and S_p denote the reactive and active power static droop gains, respectively. S_q and S_p are calculated as follows.

$$S_q = \frac{\triangle V}{Q_{DG_{max}}}, \tag{11}$$

$$S_p = \frac{\triangle \omega}{P_{DG_{max}}}, \tag{12}$$

where $\triangle w$ and $\triangle V$ denote the maximum permissible deviation of frequency and voltage, respectively; $Q_{DG_{max}}$ and $P_{DG_{max}}$ denote the maximum reactive and active capacities of the DG unit, respectively.

The following equations must be satisfied in order to share the load among DG units according to droop control.

$$S_{p,1}P_{DG,1_{max}} = S_{p,2}P_{DG,2_{max}} = \ldots = S_{p,i}P_{DG,i_{max}} \tag{13}$$

$$S_{q,1}Q_{DG,1_{max}} = S_{q,2}Q_{DG,2_{max}} = \ldots = S_{q,i}Q_{DG,i_{max}} \tag{14}$$

The active and reactive power output of a DG, operating with droop control, can be calculated as follows.

$$P_{DG,i} = \frac{1}{S_{p,i}}(\omega^* - \omega) \tag{15}$$

$$Q_{DG,i} = \frac{1}{S_{q,i}}(V_i^* - V_i) \tag{16}$$

3. Adaptive Backward/Forward Sweep Algorithm (ABFS)

There are three parts to the proposed algorithm: (1) revised backward sweep, (2) revised forward sweep, and (3) frequency and reference voltage update. Prior to moving into these steps, predefined parameters must be initialized in order to calculate PF variables' initial values.

3.1. Initialization

An angle reference (AR) bus is selected as the first step of the initialization. After that, all buses' frequencies and voltages are set to 1 pu. Both loops have a tolerance value of 1×10^{-8}.

3.2. Modified Backward Sweep

A conventional BFS algorithm starts with a backward sweep. Using the bus voltage as a known variable, this sweep computes the current of each branch. In addition to the apparent power, the voltages on the buses, and the reference voltage are all used for calculating the branch currents. The apparent injected power of PQ buses can be calculated using the following equation:

$$S_i = P_i + jQ_i = (P_{g,i} - P_{l,i}) + j(Q_{g,i} - Q_{l,i}) \tag{17}$$

The generation of active and reactive power at droop buses, however, is dependent on the system frequency and bus voltage. Droop buses are calculated using different equations shown in Equations (15)–(17):

$$S_i = \left(P^o_{g,i} + \frac{1}{S_{p,i}}(w_o - w) - P_{l,i}\right) + j\left(Q^o_{g,i} + \frac{1}{S_{q,i}}(|V_o| - |V_i|) - Q_{l,i}\right) \tag{18}$$

The apparent power is later used to determine the bus current using the following equation:

$$I_i = \left(\frac{S_i}{V_i}\right)^* \tag{19}$$

In order to calculate branch currents, the bus currents are added backward from the lower buses to the reference bus. This procedure can be expressed as follows:

$$[\mathbf{I}_{ij}] = [\mathbf{BIBC}][\mathbf{I}_i] \tag{20}$$

where the transformation matrix **BIBC** is defined in [37].

3.3. Modified Forward Sweep

By utilizing the estimated branch current of the backward sweep, the conventional BFS algorithm recalculates the bus voltages. As part of this step, branch currents and branch impedances are taken into account for calculating voltages from the AR bus (except the AR bus) to downstream buses. As a result, bus voltages can also be determined using branch impedance, reference voltage, and branch current, as shown in the equation below.

$$[\mathbf{V}] = [\mathbf{V}_{ref}] - [\mathbf{BCBV}][\mathbf{I}_{ij}] \tag{21}$$

where BCBV represents a transformation matrix, and its calculation is outlined in [37]. Here, the calculation of voltages using branch currents requires BCBV. Moreover, $[\mathbf{V}]$ and $[\mathbf{V}_{ref}]$ are the bus voltages from buses 2 to N and the AR bus, respectively.

After implementing the droop buses in the backward sweep, the current obtained may be high in some cases. As a result, the updated voltage may be far from the equilibrium value and the algorithm may diverge from the solution. To overcome this issue, a decelerate parameter must be introduced in the voltage update equation. Therefore, after introducing the deceleration parameter, β, the voltage update equation becomes:

$$[\mathbf{V}]^{k+1} = (1-\beta)[\mathbf{V}]^{k} + \beta([\mathbf{V}_{ref}] - [\mathbf{BCBV}][\mathbf{I}_{ij}]) \tag{22}$$

where the value of β must be in the range 0 to 1. k represents the iteration index used in the BFS algorithm.

3.4. Frequency and Reference Voltage Update

Essentially, this is a step that is used to correct the frequency and voltage of the AR bus. In islanded MGs, the system frequency and voltage of the AR bus are considered global variables. Thus, it is necessary to recalculate these values once the BFS algorithm has converged.

In addition to being a droop bus, the AR bus operates as an upstream bus as well. At equilibrium, the AR bus must also satisfy its droop characteristics. The voltage and system frequency of the AR bus are recalculated according to the mismatch in droop characteristics. With droop-controlled MGs, the system frequency is determined by all DGs' active power-sharing, implying that each DG acts as one unit and has a corresponding frequency droop. Based on the following equation, we can calculate the equivalent droop of the system.

$$S_{p,equ} = \sum_{i \epsilon DB} S_{p,i} \tag{23}$$

where DB is a set of all droop buses.

Then, the new system frequency can be calculated using the following equation.

$$w^{m+1} = w_o - S_{p,equ}\left(\sum_{k \epsilon DB}(P^{o}_{g,k} - P^{m+1}_{g,k})\right) \tag{24}$$

where m represents the loop index. A loop is different from an iteration in the sense that each loop may have many iterations. Due to the change in system frequency, the line reactances should also be modified as follows.

$$X^{m+1}_{ij} = w^{m+1} L_{ij} \tag{25}$$

The AR bus voltage is updated using the net imbalance of the AR bus voltage droop, $\triangle V$. We can calculate $\triangle V$ using Equation (26). A voltage update is then performed using Equation (27):

$$\triangle V^{m+1} = (V_o - |V_{AR}|^{m}) + S_{q,AR}\left(Q^{o}_{g,AR} - Q^{m+1}_{g,AR}\right) \tag{26}$$

$$V^{m+1}_{ref} = V^{m}_{ref} + \alpha \triangle V^{m+1} \tag{27}$$

where α is another deceleration factor having values between 0.3 to 1. The parameters of ABFS, α, and β are adapted using the simplex method, where the objective function is defined as the sum of all mismatches in the PF equations. The flow chart of the proposed algorithm is shown in Figure 1.

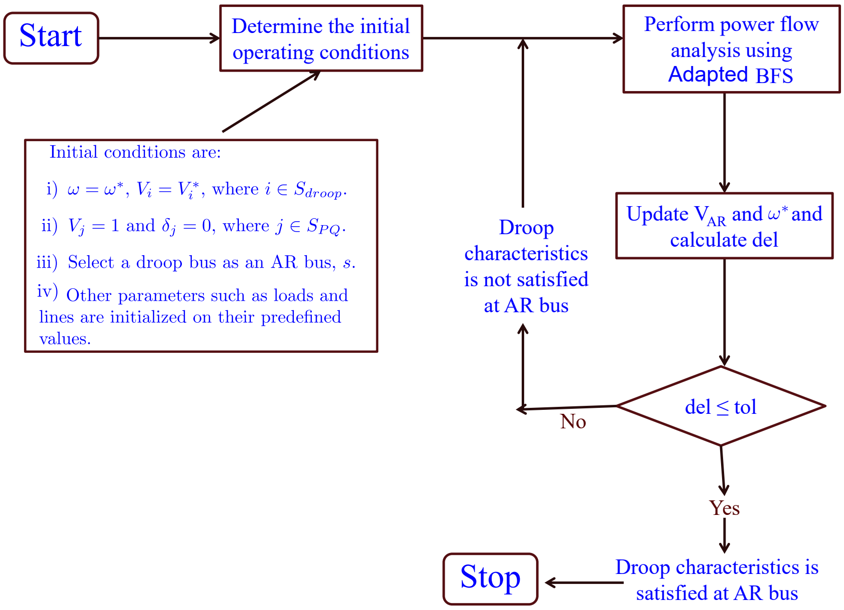

Figure 1. Flow chart of ABFS.

The main steps of ABFS are as follows:

Step 1: First, we determine the initial operating conditions of the MG. We set all PF variables as follows: $\omega = \omega^*$, $V_i = V_i^*, \forall i \in S_{droop}$ and $V_j = 1, S_j = 0, \forall j \in S_{PQ}$. Then, we select a droop bus as an AR bus, and the other parameters, such as loads and lines, are initialized on their predefined values.

Step 2: In this step, we apply ABFS to solve the power flow problem at the given ω value.

Step 3: We update the bus voltage of the AR bus and system frequency based on the obtained solution in the previous step. For this purpose, we utilize Equations (24) and (27).

Step 4: Then, we check the droop characteristics of the AR bus. If the obtained bus voltage and generated power of the AR bus are not satisfying its droop characteristics, we repeat steps 2 and 3. Otherwise, we return the previously obtained solution as the final solution.

4. Validation of Proposed Algorithm

In this section, the applicability of the proposed algorithm, NBSF, is validated on a small six-bus test system [17]. The test system is shown in Figure 2. This system is small and therefore can easily be simulated in the environment of the well-accepted simulation tool PSCAD/EMTDC. Therefore, to illustrate the accuracy of results obtained using the proposed algorithm, the results were compared with those obtained from the time-domain model [38,39] of the test system. NBSF was realized in MATLAB for solving the load flow problem. The time-domain model of the test system was simulated in PSCAD/EMTDC software and the required system data are given in Table 2. The obtained results of these methods are reported in Table 3. It is clearly seen from Table 3 that the maximum error between these two methods was much smaller. However, to achieve the final solution, NBSF took an execution time of approximately 0.009 s which was much less compared to the required simulation time of PSCAD. The agreement between the solutions obtained from both methods proved the accuracy of NBSF and significantly reduced the execution time to achieve the final solution proving the efficiency of NBSF in solving the PF problem of IDRACMs.

Further, to show the weakness of other backward–forward sweep algorithms (viz., DBFS and MBFS) in case of application to IDRACMs, a detailed comparison of the performance of ABFS, DBFS, and MBFS is also discussed in the next section.

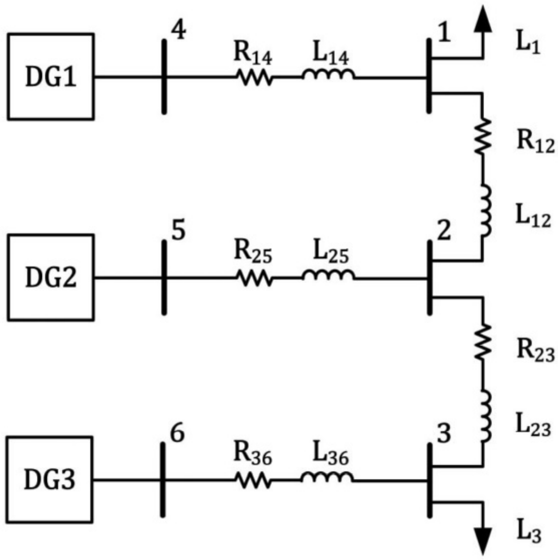

Figure 2. Six-bus MG [17].

Table 2. Data required for modeling the six-bus test system in the time domain.

$1/S_p$ (rad/s/W)	**$1/S_q$ (V/VAR)**	**w^* (rad/s)**	**V^* (V)**
9.4×10^{-5}	1.3×10^{-3}	377	127
Line parameters			
From bus	To bus	R_{line} (Ω)	L_{line} (mH)
1	2	0.43	0.32
1	4	0.30	0.35
2	5	0.20	0.25
2	3	0.15	1.84
3	6	0.05	0.05
Load parameter			
Bus number	R_{load} (Ω)	L_{load} (mH)	
1	6.95	12.20	
3	5.01	9.40	

Table 3. Validation of obtained result of the six-bus test system.

Bus	**Voltage Magnitude (V)**		**Angle (rad)**	
	PSCAD	**NICINR**	**PSCAD**	**NICINR**
1	121.92	121.92	0.0078	0.0078
2	123.51	123.51	−0.0013	−0.0013
3	122.42	122.42	−0.0388	−0.0389
4	125.37	125.37	0.0065	0.0065
5	125.74	125.74	0 *	0 *
6	123.11	123.10	−0.0420	−0.0421
Err.	0.0081%		0.26%	
Freq.	376.6645	376.6645		
Time	172 s	0.009 s		

*: Angle Reference bus.

5. Comparison with DBFS and MBFS

Here, we compare the proposed algorithm's outcome with that of MBFS [21] and DBFS [20] for a 33-bus radial distribution test system, named case33. In order to make a fair comparison, we directly used the test settings and droop parameters from [20,21]. Furthermore, we also took the results of PSCAD/EMTDC into consideration for the evaluation.

In Table 4, we depict the results of ABFS and PSCAD/EMTDC along with results presented in [20,21]. We set each DG's nominal power setting at $0.9 + j0.9$ per unit for a fair comparison. Table 4 reports the apparent power that was calculated by taking the sum of the nominal power and the power generated by the droop-based DG. The results of Table 4 show that all algorithms achieved similar system frequencies, whereas the bus voltage magnitudes differed. To emphasize the significance of this result, we report the real, reactive, and maximum voltage magnitudes mismatch in Table 4. To calculate the mismatch, we took PSCAD/EMTDC's result as the true solution to the PF problem. In Table 4, it is evident that the ABFS's solution was more comparable to PSCAD/EMTDC than to other methods as follows:

(i) *Voltage magnitude:* For buses 1, 5, 12, 13, 15, 16, 17, 28, 29, 31, and 32, DBFS delivered inaccurate voltage magnitudes. MBFS returned inaccurate solutions for buses 13, 22, 27, and 30. In contrast, ABFS provided accurate bus voltages for all buses. As a result, we can conclude that ABFS calculated bus voltages with a higher level of accuracy than other methods.

(ii) *Active and reactive generation:* DBFS provided inaccurate solutions in all droop buses such as buses 1, 6, 13, 25, and 33.

Therefore, ABFS produced more accurate outcomes than MBFS or DBFS.

With DBFS, the estimated reactive power at DGs was slightly different than with MBFS or ABFS. There is a good explanation for it in [21], so there is no need to discuss it here. Meanwhile, ABFS and MBFS fully incorporated the DG's droop characteristic in their structure, resulting in values that were closer to the values of PSCAD/EMTDC.

For a further analysis of the differences among ABFS, MBFS, and DBFS performance, we show the dynamics of the AR bus's voltage magnitude frequency and operating system frequency with time in Figure 3. According to this figure, ABFS required much less computation time to converge than DBFS and MBFS. It is important to note that the main reason for the disparity in computation time and dynamics is due to variations in the algorithms' basic structure. To accommodate the droop characteristics of the DG connected to the reference bus, the system frequency and voltage magnitude of the reference bus is revised in a loop in ABFS. In the backward sweep step of BSF, ABFS updates the generated power to account for the other DGs' droop characteristics. Compared to MBFS and DBFS, ABSF's structure minimizes computation burden, speeding convergence, due to the fact that MBFS and DBFS recalculate the generated power of all droop-controlled DGs beyond the scope of BSF's loop. To compute the real and reactive power individually in DBFS, separate loops are employed, increasing the computational burden and convergence time. As shown in Figure 3, the variations of AR's voltage magnitude and system frequency were considerably larger with DBFS. As a result of the oscillatory behavior of the DBFS and MBFS algorithms, these cannot achieve convergence quickly and are also unreliable in difficult PF problems. Based on the outlined points, it can be concluded that ABFS has a higher efficiency and higher robustness than DBFS and MBFS.

Table 4. ABFS algorithm versus DBFS, MBFS, and PSCAD/EMTDC results for case33.

Bus	**Voltage Magnitude (pu)**				**Active Load (pu)**				**Reactive Load (pu)**			
	DBFS	**MBFS**	**PSCAD**	**ABFS**	**DBFS**	**MBFS**	**PSCAD**	**ABFS**	**DBFS**	**MBFS**	**PSCAD**	**ABFS**
1	0.996	0.997	0.997	0.997	0.00	0.00	0.00	0.00	0.00	0.00	0.00	0.00
2	0.996	0.996	0.996	0.996	0.20	0.20	0.20	0.20	0.12	0.12	0.12	0.12
3	0.993	0.993	0.993	0.993	0.18	0.18	0.18	0.18	0.08	0.08	0.08	0.08
4	0.992	0.992	0.992	0.992	0.24	0.24	0.24	0.24	0.16	0.16	0.16	0.16
5	0.991	0.992	0.992	0.992	0.12	0.12	0.12	0.12	0.06	0.06	0.06	0.06
6	0.991	0.991	0.991	0.991	0.12	0.12	0.12	0.12	0.04	0.04	0.04	0.04
7	0.990	0.990	0.990	0.990	0.40	0.40	0.40	0.40	0.20	0.20	0.20	0.20
8	0.990	0.990	0.990	0.990	0.40	0.40	0.40	0.40	0.20	0.20	0.20	0.20
9	0.992	0.992	0.992	0.992	0.12	0.12	0.12	0.12	0.04	0.04	0.04	0.04
10	0.994	0.994	0.994	0.994	0.12	0.12	0.12	0.12	0.04	0.04	0.04	0.04
11	0.995	0.995	0.995	0.995	0.09	0.09	0.09	0.09	0.06	0.06	0.06	0.06
12	0.996	0.995	0.995	0.995	0.12	0.12	0.12	0.12	0.07	0.07	0.07	0.07
13	1.001	1.001	1.000	1.000	0.12	0.12	0.12	0.12	0.07	0.07	0.07	0.07
14	0.999	0.999	0.999	0.999	0.24	0.24	0.24	0.24	0.16	0.16	0.16	0.16
15	0.998	0.997	0.997	0.997	0.12	0.12	0.12	0.12	0.02	0.02	0.02	0.02
16	0.997	0.996	0.996	0.996	0.12	0.12	0.12	0.12	0.04	0.04	0.04	0.04
17	0.995	0.994	0.994	0.994	0.12	0.12	0.12	0.12	0.04	0.04	0.04	0.04
18	0.994	0.994	0.994	0.994	0.18	0.18	0.18	0.18	0.08	0.08	0.08	0.08
19	0.995	0.995	0.995	0.995	0.18	0.18	0.18	0.18	0.08	0.08	0.08	0.08
20	0.992	0.992	0.992	0.992	0.18	0.18	0.18	0.18	0.08	0.08	0.08	0.08
21	0.991	0.991	0.991	0.991	0.18	0.18	0.18	0.18	0.08	0.08	0.08	0.08
22	0.990	0.991	0.990	0.990	0.18	0.18	0.18	0.18	0.08	0.08	0.08	0.08
23	0.992	0.992	0.992	0.992	0.18	0.18	0.18	0.18	0.10	0.10	0.10	0.10
24	0.990	0.990	0.990	0.990	0.84	0.84	0.84	0.84	0.40	0.40	0.40	0.40
25	0.991	0.991	0.991	0.991	0.84	0.84	0.84	0.84	0.40	0.40	0.40	0.40
26	0.990	0.990	0.990	0.990	0.12	0.12	0.12	0.12	0.05	0.05	0.05	0.05
27	0.989	0.990	0.989	0.989	0.12	0.12	0.12	0.12	0.05	0.05	0.05	0.05
28	0.985	0.986	0.986	0.986	0.12	0.12	0.12	0.12	0.04	0.04	0.04	0.04
29	0.983	0.984	0.984	0.984	0.24	0.24	0.24	0.24	0.14	0.14	0.14	0.14
30	0.983	0.984	0.983	0.983	0.40	0.40	0.40	0.40	1.20	1.20	1.20	1.20
31	0.985	0.986	0.986	0.986	0.30	0.30	0.30	0.30	0.14	0.14	0.14	0.14
32	0.987	0.988	0.988	0.988	0.42	0.42	0.42	0.42	0.20	0.20	0.20	0.20
33	0.990	0.990	0.990	0.990	0.12	0.12	0.12	0.12	0.08	0.08	0.08	0.08
Max Error	0.001	0.001	–	0.000	0.00	0.00		0.00	0.00	0.00		0.00
					Active Generation (pu)				Reactive Generation (pu)			
1	0.996	0.997	0.997	0.997	2.494	2.502	2.502	2.502	0.978	0.967	0.967	0.967
6	0.991	0.991	0.991	0.991	0.981	0.980	0.980	0.980	0.904	0.909	0.909	0.909
13	1.001	1.001	1.000	1.000	1.707	1.701	1.701	1.701	0.931	0.893	0.893	0.893
25	0.991	0.991	0.991	0.991	0.981	0.980	0.980	0.980	0.904	0.909	0.909	0.909
33	0.990	0.990	0.990	0.990	1.304	1.301	1.300	1.300	0.916	0.948	0.948	0.948
Max Error	0.001	0.001		0.000	0.008	0.001		0.000	0.038	0.000		0.000
					Pg	Qg	Pl	Ql	Ploss	Qloss	Freq.	CT(s)
				DBFS	7.467	4.633	7.430	4.600	0.037	0.033	0.919	0.521
				MBFS	7.464	4.626	7.430	4.600	0.034	0.026	0.920	0.165
				PSCAD	7.463	4.625	7.430	4.600	0.035	0.027	0.920	462.142
				ABFS	7.463	4.625	7.430	4.600	0.035	0.027	0.920	0.018

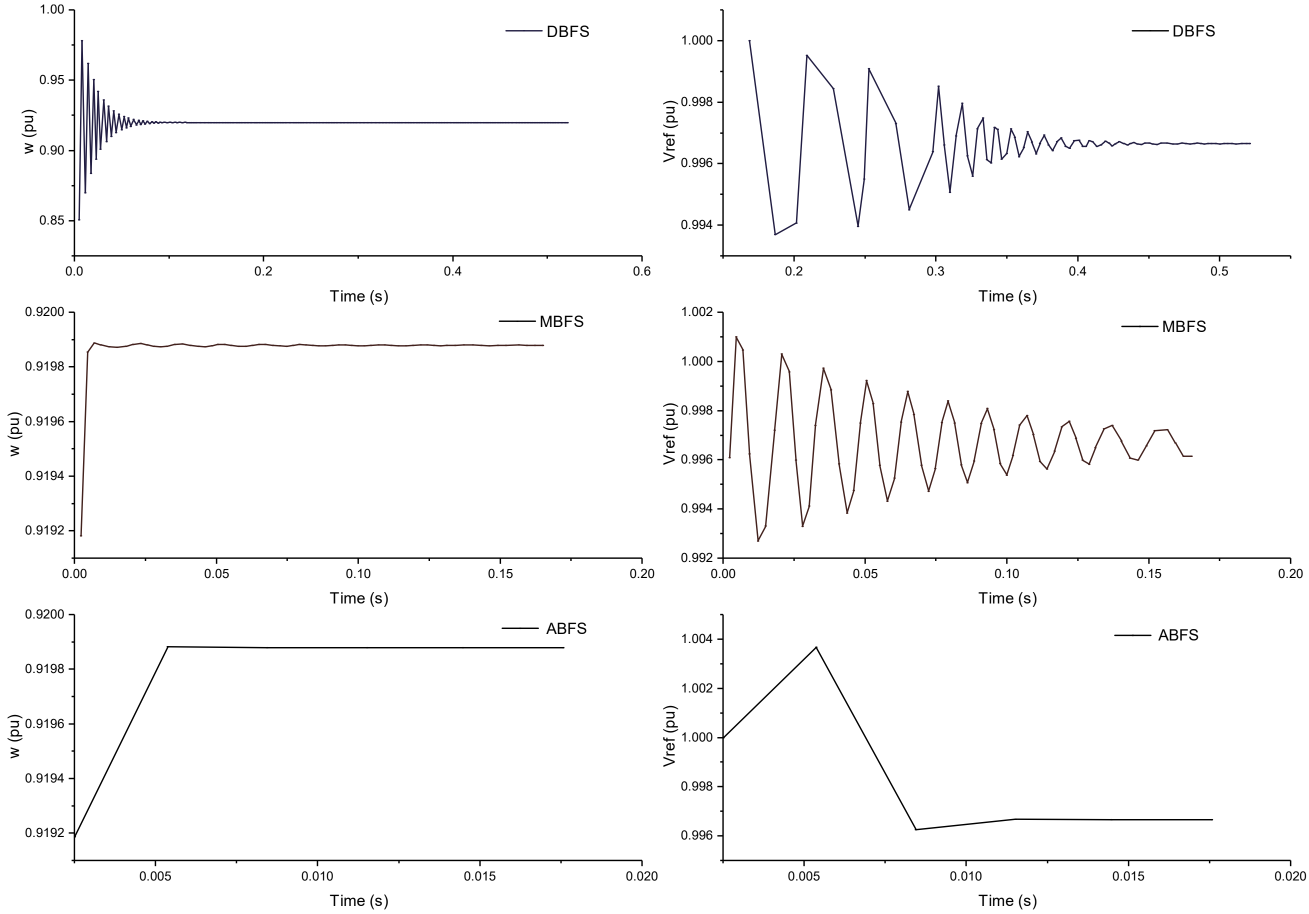

Figure 3. Convergence of the solution with respect to computation time.

6. Comparison with NTR and MNR

This section compares the performance of the ABFS algorithm with Jacobian algorithms, namely, MNR and NTR, in order to establish its robustness.

We utilized three test systems, viz., case22, case38, and case69, as test systems for analyzing the performance of MBFS, DBFS, MNR, and NTR. These test systems are described in their reported papers [40–42], respectively, and Table 5 contains the data of the droop-controlled DGs. In Table 6, we present the convergence time for DBFS, MBFS, NTR, and MNR. Table 6 clearly illustrates that both DBFS and MBFS did not converge on a single test case because of their dynamics characteristics. In all test systems, ABFS required less time to converge than MNR and NTR because (i) the Jacobian matrix was not needed to improve the solution, which was a computationally intensive procedure, (ii) the bus admittance matrix was computed at each iteration in the NTR and MNR algorithms, while the bus admittance matrix was not computed in the ABFS algorithm. Furthermore, for case69, MNR did not converge at its solution since it took place at the intersection of the unsolvable and solvable subregions.

Table 5. Droop gains, nominal values, and operative mode of DGs and Q_{max} limit for the case22, case38, and case69 test systems.

Test System	Bus Number	$1/S_p$	$1/S_q$	ω^*	$\lvert V_0^* \rvert$	Q_{max}
case22	5	0.005102	0.05	1	1	0.2
	13	0.001502	0.03	1	1	0.3
	15	0.004506	0.01	1	1	0.4
	21	0.001502	0.02	1	1	0.4
case38	34	0.005102	0.02	1	1.01	0.9
	35	0.001502	0.03333	1	1.01	0.6
	36	0.004506	0.02	1	1.01	0.9
	37	0.002253	0.05	1	1.01	0.3
	38	0.002253	0.05	1	1.01	0.3
case69	1	0.005102	0.05	1	1.01	0.35
	25	0.004506	0.05	1	1.01	0.45
	29	0.002253	0.01	1	1.01	0.9
	50	0.002253	0.1	1	1.01	0.6
	60	0.005102	0.1	1	1.01	1.5
	65	0.001502	0.03	1	1.01	0.9

Table 6. Computation time required to solve power flow for case22, case38, and case69 considering the ABFS, MNR, NTR, MBFS, and DBFS algorithms. (NC: not converged).

System	ABFS	MNR	NTR	MBFS	DBFS
22-bus	4.96×10^{-3}	6.35×10^{-2}	1.77×10^{-2}	NC	NC
38-bus	3.01×10^{-2}	1.46×10^{-1}	3.48×10^{-2}	NC	NC
69-bus	4.33×10^{-2}	NC	1.43×10^{-1}	NC	NC

7. Discussion

We compared ABFS's performance to that of NTR, MNR, DBFS, and MBFS over four test systems. DBFS and MBFS succeeded in solving the PF problem on only the case33 test systems. Therefore, in the case of the case33 test system, ABFS's performance could only be assessed against DBFS and MBFS. ABFS appeared to be more robust and rigorous than DBFS and MBFS.

We previously pointed out that the major factor contributing to the divergence of DBFS and MBFS was the fluctuations in the voltage magnitude and frequency of the reference bus. In order to demonstrate this behavior, DBFS and MBFS were implemented on a simple six-bus test system. In the case of DBFS and MBFS, all droop-controlled DGs produced reactive power outside of their solvable range, leading to a divergence of the DBFS and MBFS algorithms. Meanwhile, ABFS incorporated the deacceleration factors α and β to dampen the oscillation of system variables. Therefore, the ABFS algorithm was able to reach a smooth convergence when solving hard problems.

The Jacobian-based algorithms MNR and NTR both required an admittance matrix to improve their solutions. With the increasing system size, the Jacobian matrix inverse became more computationally expensive. The impact of this burden on computing was also presented in Table 6. As shown in that table, with the increase in system size, the computation time needed to converge also increased heavily. In addition to the Jacobian matrix inverse calculations, admittance matrix calculations at each iteration also contributed to computational complexity. ABFS did not require these intensive computations, so it converged faster than Jacobian-based algorithms. Further, the system size had little effect on ABFS computation time, as illustrated in Table 6.

8. Conclusions

This paper presented an algorithm to solve the power flow problem of islanded droop-regulated AC microgrids. This algorithm, named ABFS, was a variant of the well-known BFS algorithm, which is extensively applied to the power flow analysis of distribution networks that are connected to the main grid. It is important to note that our method did not require the utilization of a slack bus that had a preset voltage and infinite power capability. A methodology for updating the voltage and frequency deviations resulting from the backward to forward sweep was proposed based on the droop functions. Following each forward sweep, this update was distributed to every node, thus allowing power and bus voltages to be modified via the droop function of each generation unit. Furthermore, two adaptive deceleration factors were introduced to dampen the dynamics of the variables. We compared the performance of ABFS against two other BFS variants, DBFS and MBFS, in order to assess its consistency and effectiveness. Moreover, algorithms involving the Jacobian, viz., NTR and MNR, were also included in the comparative analysis. It was found that ABFS converged faster than other algorithms without compromising accuracy. We also discussed how we could boost the speed of the algorithm by defining the initial guess in a closed form. In general, the algorithm shared the same characteristics as other grid-connected BFS methods, and by taking into account the network characteristics of islanded microgrids, it enabled a more thorough analysis of islanded microgrids. In order to validate the consistency of the solution, we compared the performance of the proposed algorithm against the time-domain simulation of test systems in PSCAD/EMTDC. It is evident from the results that ABFS yielded accurate solutions.

Author Contributions: Conceptualization, A.K. (Abhishek Kumar) and A.K. (Abhimanyu Kumar); software, A.K. (Abhimanyu Kumar) and A.K. (Abhishek Kumar); validation, R.M. and D.-G.L.; formal analysis, A.K. (Abhishek Kumar) and R.M.; investigation, A.K. (Abhimanyu Kumar) and D.-G.L.; resources, R.M. and D.-G.L.; data curation, A.K. (Abhimanyu Kumar) and A.K. (Abhishek Kumar); writing—original draft preparation, A.K. (Abhimanyu Kumar) and A.K. (Abhishek Kumar); writing—review and editing, R.M. and D.-G.L.; visualization, A.K. (Abhimanyu Kumar) and A.K. (Abhishek Kumar); supervision, R.M. and D.-G.L. All authors have read and agreed to the published version of the manuscript.

Funding: This work was supported by the Basic Science Research Program through the National Research Foundation of Korea (NRF) funded by the Ministry of Education (2021R1I1A3049810) and National Research Foundation of Korea (NRF) grant funded by the Korean Government (MSIT) (No. 2021R1C1C1012590) and (No. NRF-2022R1A4A1023248).

Data Availability Statement: Not applicable.

Conflicts of Interest: The authors declare no conflict of interest.

References

1. Cheng, C.S.; Shirmohammadi, D. A three-phase power flow method for real-time distribution system analysis. *IEEE Trans. Power Syst.* **1995**, *10*, 671–679. [CrossRef]
2. Lisboa, A.; Guedes, L.; Vieira, D.; Saldanha, R. A fast power flow method for radial networks with linear storage and no matrix inversions. *Int. J. Electr. Power Energy Syst.* **2014**, *63*, 901–907. [CrossRef]
3. Birt, K.A.; Graffy, J.J.; McDonald, J.D.; El-Abiad, A.H. Three phase load flow program. *IEEE Trans. Power Appar. Syst.* **1976**, *95*, 59–65. [CrossRef]
4. Garcia, A.; Zago, M. Three-phase fast decoupled power flow for distribution networks. *IEE Proc.-Gener. Transm. Distrib.* **1996**, *143*, 188–192. [CrossRef]
5. Zhang, X.P. Fast three phase load flow methods. *IEEE Trans. Power Syst.* **1996**, *11*, 1547–1554. [CrossRef]
6. Le Nguyen, H. Newton-Raphson method in complex form [power system load flow analysis]. *IEEE Trans. Power Syst.* **1997**, *12*, 1355–1359. [CrossRef]
7. Zhang, F.; Cheng, C.S. A modified Newton method for radial distribution system power flow analysis. *IEEE Trans. Power Syst.* **1997**, *12*, 389–397. [CrossRef]

8. Luo, G.X.; Semlyen, A. Efficient load flow for large weakly meshed networks. *IEEE Trans. Power Syst.* **1990**, *5*, 1309–1316. [CrossRef]
9. Shirmohammadi, D.; Hong, H.W.; Semlyen, A.; Luo, G. A compensation-based power flow method for weakly meshed distribution and transmission networks. *IEEE Trans. Power Syst.* **1988**, *3*, 753–762. [CrossRef]
10. Wu, W.; Zhang, B. A three-phase power flow algorithm for distribution system power flow based on loop-analysis method. *Int. J. Electr. Power Energy Syst.* **2008**, *30*, 8–15. [CrossRef]
11. Chen, T.H.; Yang, N.C. Loop frame of reference based three-phase power flow for unbalanced radial distribution systems. *Electr. Power Syst. Res.* **2010**, *80*, 799–806. [CrossRef]
12. Kamh, M.Z.; Iravani, R. Unbalanced model and power-flow analysis of microgrids and active distribution systems. *IEEE Trans. Power Deliv.* **2010**, *25*, 2851–2858. [CrossRef]
13. Olivares, D.E.; Mehrizi-Sani, A.; Etemadi, A.H.; Cañizares, C.A.; Iravani, R.; Kazerani, M.; Hajimiragha, A.H.; Gomis-Bellmunt, O.; Saeedifard, M.; Palma-Behnke, R.; et al. Trends in microgrid control. *IEEE Trans. Smart Grid* **2014**, *5*, 1905–1919. [CrossRef]
14. Bompard, E.; Carpaneto, E.; Chicco, G.; Napoli, R. Convergence of the backward/forward sweep method for the load-flow analysis of radial distribution systems. *Int. J. Electr. Power Energy Syst.* **2000**, *22*, 521–530. [CrossRef]
15. Eminoglu, U.; Hocaoglu, M.H. Distribution systems forward/backward sweep-based power flow algorithms: A review and comparison study. *Electr. Power Compon. Syst.* **2008**, *37*, 91–110. [CrossRef]
16. Nikkhajoei, H.; Iravani, R. Steady-state model and power flow analysis of electronically-coupled distributed resource units. *IEEE Trans. Power Deliv.* **2007**, *22*, 721–728. [CrossRef]
17. Abdelaziz, M.M.A.; Farag, H.E.; El-Saadany, E.F.; Mohamed, Y.A.R.I. A novel and generalized three-phase power flow algorithm for islanded microgrids using a newton trust region method. *IEEE Trans. Power Syst.* **2013**, *28*, 190–201. [CrossRef]
18. Mumtaz, F.; Syed, M.; Al Hosani, M.; Zeineldin, H. A novel approach to solve power flow for islanded microgrids using modified newton raphson with droop control of dg. *IEEE Trans. Sustain. Energy* **2016**, *7*, 493–503. [CrossRef]
19. Moghaddas-Tafreshi, S.; Mashhour, E. Distributed generation modeling for power flow studies and a three-phase unbalanced power flow solution for radial distribution systems considering distributed generation. *Electr. Power Syst. Res.* **2009**, *79*, 680–686. [CrossRef]
20. Díaz, G.; Gómez-Aleixandre, J.; Coto, J. Direct backward/forward sweep algorithm for solving load power flows in AC droop-regulated microgrids. *IEEE Trans. Smart Grid* **2016**, *7*, 2208–2217. [CrossRef]
21. Hameed, F.; Al Hosani, M.; Zeineldin, H. A modified backward/forward sweep load flow method for islanded radial microgrids. *IEEE Trans. Smart Grid* **2017**, *10*, 910–918. [CrossRef]
22. Ju, Y.; Wang, J.; Zhang, Z.; Huang, Y.; Lin, Y. A Calculation Method for Three-Phase Power Flow in Micro-Grid Based on Smooth Function. *IEEE Trans. Power Syst.* **2020**, *35*, 4896–4903. [CrossRef]
23. Kumar, A.; Jha, B.K.; Das, S.; Mallipeddi, R. Power flow analysis of islanded microgrids: A differential evolution approach. *IEEE Access* **2021**, *9*, 61721–61738. [CrossRef]
24. Nazari, A.A.; Keypour, R.; Beiranvand, M.; Amjady, N. A decoupled extended power flow analysis based on Newton-Raphson method for islanded microgrids. *Int. J. Electr. Power Energy Syst.* **2020**, *117*, 105705. [CrossRef]
25. Kumar, A.; Jha, B.K.; Dheer, D.K.; Misra, R.K.; Singh, D. A Nested-Iterative Newton-Raphson based Power Flow Formulation for Droop-based Islanded Microgrids. *Electr. Power Syst. Res.* **2020**, *180*, 106131. [CrossRef]
26. Pan, Z.; Wu, J.; Ding, T.; Liu, J.; Wang, F.; Tong, X. Load flow calculation for droop-controlled islanded microgrids based on direct Newton–Raphson method with step size optimisation. *IET Gener. Transm. Distrib.* **2020**, *14*, 4775–4787. [CrossRef]
27. Tostado-Véliz, M.; Kamel, S.; Jurado, F. Power flow approach based on the S-iteration process. *IEEE Trans. Power Syst.* **2020**, *35*, 4148–4158. [CrossRef]
28. Kumar, A.; Das, S.; Mallipeddi, R. An Inversion-Free Robust Power-Flow Algorithm for Microgrids. *IEEE Trans. Smart Grid* **2021**, *12*, 2844–2859. [CrossRef]
29. Bayat, M.; Koushki, M.M.; Ghadimi, A.A.; Tostado-Véliz, M.; Jurado, F. Comprehensive enhanced Newton Raphson approach for power flow analysis in droop-controlled islanded AC microgrids. *Int. J. Electr. Power Energy Syst.* **2022**, *143*, 108493. [CrossRef]
30. Bai, H.; Tang, X.; Yuan, Z.; Li, Q.; Pan, S.; Deng, P.; Zhou, C.; Luo, N. A novel three-phase unbalanced power flow solution for islanded microgrids with distributed generations under droop controls. *Energy Rep.* **2022**, *8*, 1438–1447. [CrossRef]
31. Elgamal, M.; Korovkin, N.; Menaem, A.A.; Elmitwally, A. An algorithm for power flow analysis in isolated hybrid energy microgrid considering DG droop model and virtual impedance control loop. *Sustain. Energy Grids Netw.* **2022**, *32*, 100875. [CrossRef]
32. Raj, R.; Babu, P.S. A Backward/Forward Method for Solving Load Flows in Droop-Controlled Microgrids. In *Control Applications in Modern Power System*; Springer: Berlin/Heidelberg, Germany, 2021; pp. 367–377.
33. Vilaisarn, Y.; Abdelaziz, M. An inversion-free sparse Zbus power flow algorithm for large-scale droop controlled islanded microgrids. *Int. J. Electr. Power Energy Syst.* **2020**, *121*, 106048. [CrossRef]
34. Bayat, M.; Ghaseminezhad, K.; Ghadimi, A.A. An efficient iterative approach for power flow solution of droop-controlled islanded AC microgrids through conventional methods. *Int. J. Electr. Power Energy Syst.* **2021**, *130*, 106962. [CrossRef]
35. Lu, F.; Liu, H. An Accurate Power Flow Method for Microgrids with Conventional Droop Control. *Energies* **2022**, *15*, 5841. [CrossRef]

36. Rashidirad, N.; Mahseredjian, J.; Kocar, I.; Karaagac, U.; Saad, O. MANA-Based Load-Flow Solution for Islanded AC Microgrids. *IEEE Trans. Smart Grid* **2022**. [CrossRef]
37. Teng, J.H. A direct approach for distribution system load flow solutions. *IEEE Trans. Power Deliv.* **2003**, *18*, 882–887. [CrossRef]
38. Mohamed, Y.A.R.I.; El-Saadany, E.F. Adaptive decentralized droop controller to preserve power sharing stability of paralleled inverters in distributed generation microgrids. *IEEE Trans. Power Electron.* **2008**, *23*, 2806–2816. [CrossRef]
39. Pogaku, N.; Prodanovic, M.; Green, T.C. Modeling, analysis and testing of autonomous operation of an inverter-based microgrid. *IEEE Trans. Power Electron.* **2007**, *22*, 613–625. [CrossRef]
40. Raju, M.R.; Murthy, K.R.; Ravindra, K. Direct search algorithm for capacitive compensation in radial distribution systems. *Int. J. Electr. Power Energy Syst.* **2012**, *42*, 24–30. [CrossRef]
41. Singh, D.; Misra, R.; Singh, D. Effect of load models in distributed generation planning. *IEEE Trans. Power Syst.* **2007**, *22*, 2204–2212. [CrossRef]
42. Das, D. Optimal placement of capacitors in radial distribution system using a Fuzzy-GA method. *Int. J. Electr. Power Energy Syst.* **2008**, *30*, 361–367. [CrossRef]